

Graviton- and Inflaton-mediated Dark Matter Production after Large Field Polynomial Inflation

Nicolás Bernal,^a Julia Harz,^b Martin A. Mojahed^{b,c} and Yong Xu^b

^a*New York University Abu Dhabi*

PO Box 129188, Saadiyat Island, Abu Dhabi, United Arab Emirates

^b*PRISMA⁺ Cluster of Excellence and Mainz Institute for Theoretical Physics*

Johannes Gutenberg University, 55099 Mainz, Germany

^c*Physik Department, TUM School of Natural Sciences, TU München,*

James-Franck-Straße, D-85748 Garching, Germany

E-mail: nicolas.bernal@nyu.edu, julia.harz@uni-mainz.de,

mojahedm@uni-mainz.de, yonxu@uni-mainz.de

ABSTRACT: Polynomial inflation is a simple cosmological scenario, which fits the cosmic microwave background data well. It provides testable predictions for the tensor-to-scalar ratio and the running of the spectral index. In this work, we investigate the production of Dirac dark matter (DM) within the framework of large-field polynomial inflation. We study all relevant production channels including *i*) non-thermal production through inflaton decays and scatterings, and *ii*) thermal production from scattering of standard model particles mediated by inflatons and gravitons. In contrast to small-field polynomial inflation, where inflaton decay dominates DM production, we find that graviton-mediated processes can be dominant in the large-field scenario. In particular, graviton-mediated scatterings can account for the observed relic abundance even when DM is up to one order of magnitude heavier than the inflaton. For DM lighter than the inflaton, we demonstrate that the interplay between graviton- and inflaton-mediated production channels give rise to non-trivial relations between the DM mass and the reheating temperature required to account for the DM relic abundance.

Contents

| | | |
|----------|-----------------------------------|-----------|
| 1 | Introduction | 1 |
| 2 | Model Setup | 2 |
| 3 | Inflation and (P)reheating | 3 |
| 3.1 | Polynomial Inflation | 3 |
| 3.2 | (P)reheating | 5 |
| 4 | Dark Matter Production | 9 |
| 4.1 | Inflaton Decay | 11 |
| 4.2 | Inflaton Scattering | 12 |
| 4.3 | SM Particles Scattering | 13 |
| 4.3.1 | Graviton Mediation | 13 |
| 4.3.2 | Inflaton Mediation | 14 |
| 4.4 | Combined analysis | 16 |
| 5 | Conclusions | 18 |
| A | Gravitational Scattering | 18 |

1 Introduction

Cosmic inflation is an established paradigm for solving the horizon and flatness problem of standard cosmology [1–4]. The simplest inflationary scenario is the so-called slow roll (SR) single-field inflation, where a scalar inflaton field ϕ slowly rolls down its potential [5]. For the minimal SR model with a monomial potential $V(\phi) \propto \phi^p$, the most recent cosmic microwave background (CMB) experiments [6, 7] have ruled out scenarios with $p \geq 1/2$, since such potentials are too steep and yield too large tensor-to-scalar ratios r . Moreover, according to the latest Planck data [6], the most favored single-field inflation models within the Einstein gravity framework are those with concave potentials $V''(\phi) < 0$.

As a simple extension of the monomial paradigm, one can consider a renormalizable polynomial potential with a concave shape that contains a quadratic, cubic, and a quartic term [8–17]. The cosmic inflationary dynamics of this model, as well as the parameter space that is in agreement with CMB data, have recently been studied in the context of small- and large-field excursions (Refs. [18] and [19], respectively). After the end of inflation, the energy density contained in the inflaton field has to be transferred to standard-model (SM) degrees of freedom to generate the SM thermal plasma, for instance via inflaton decays into SM particles. Interestingly, in the small-field realization of the model, the reheating

temperature is typically smaller than the inflaton mass, while in the large-field realization it can be much higher.

It is well known that physics beyond the standard model (BSM) is required to explain both the existence of dark matter (DM) and the dynamical generation of the baryon asymmetry of the Universe. In the context of polynomial inflation, a rather large parameter space was found for both thermal and non-thermal baryogenesis via leptogenesis [20, 21]. DM can be produced by several processes, including non-thermal production from inflaton decays and scatterings, and thermal production from inflaton- and graviton-mediated scatterings of SM particles in the thermal plasma. In the context of small-field polynomial inflation, the generation of fermionic DM was investigated in Ref. [22] where it was shown that inflaton decays dominate over all other production channels due to radiative constraints on the reheating temperature T_{rh} , where the latter can be at most $T_{\text{rh}} \sim \mathcal{O}(10^{11})$ GeV.

In this work, we extend the previous work [22] by considering a large-field setup. In this case, radiative corrections to the inflaton potential do not place strong constraints on reheating, leading to reheating temperatures as high as $T_{\text{rh}} \sim \mathcal{O}(10^{14})$ GeV [19]. In contrast to the previously studied small-field case, we find that DM production channels mediated by gravity or the inflaton can become important. Here we present a detailed account of the interplay of DM production via gravity-mediated processes and inflation decays and scatterings. Although the current analysis is focused on polynomial inflation, our formalism can be applied to other large-field inflation models such as Starobinsky inflation [1], Higgs inflation [23] or attractor models [24].

The outline of this paper is as follows. We introduce the model setup in Section 2. The dynamics of inflation and (p)reheating are discussed in Section 3. It will set the stage for the main focus of this work, the production of DM, which is investigated in Section 4. Here, we analyze all possible production channels and the corresponding parameter space to successfully explain the DM abundance. We summarize our findings in Section 5.

2 Model Setup

Inspired by Occam’s razor, and the necessity of new physics explaining the primordial evolution of the Universe and DM, we extend the SM of particle physics with two new states, which account for the inflaton and DM. The action S of the model can be written as follows [22]

$$S = \int d^4x \sqrt{-g} (\mathcal{L}_{\text{EH}} + \mathcal{L}_{\text{SM}} + \mathcal{L}_\phi + \mathcal{L}_{\text{DM}} + \mathcal{L}_{H\phi}), \quad (2.1)$$

where g is the determinant of the Friedmann-Lemaître-Robertson-Walker metric defined by $g_{\mu\nu} = \text{diag}(1, -a^2, -a^2, -a^2)$, and a is the cosmic scale factor. \mathcal{L}_{EH} denotes the Einstein-Hilbert Lagrangian density given by

$$\mathcal{L}_{\text{EH}} = \frac{M_P^2}{2} R, \quad (2.2)$$

where R denotes the Ricci scalar and $M_P \simeq 2.4 \times 10^{18}$ GeV is the reduced Planck mass. \mathcal{L}_{SM} is the usual SM Lagrangian and \mathcal{L}_ϕ encodes the inflaton dynamics

$$\mathcal{L}_\phi = \frac{1}{2} \partial_\mu \phi \partial^\mu \phi - V(\phi). \quad (2.3)$$

The inflaton ϕ is a real scalar field, and we consider the most general renormalizable potential¹

$$V(\phi) = b\phi^2 + c\phi^3 + d\phi^4. \quad (2.4)$$

Additionally, we assume that DM is a Dirac fermion χ with the Lagrangian density²

$$\mathcal{L}_{\text{DM}} = -y_\chi \phi \bar{\chi} \chi + m_\chi \bar{\chi} \chi, \quad (2.5)$$

where y_χ denotes the Yukawa coupling to the inflaton and m_χ denotes the DM mass. The reheating of the Universe is controlled by interactions of ϕ with the SM Higgs doublet H

$$\mathcal{L}_{H\phi} = -\mu \phi H^\dagger H - \frac{1}{2} \lambda_{\phi H} \phi^2 H^\dagger H. \quad (2.6)$$

In this setup, gravitational interactions are also relevant. Expanding the metric in Eq. (2.1) around a flat Minkowski background $\eta_{\mu\nu}$ as $g_{\mu\nu} \simeq \eta_{\mu\nu} + (2/M_P) h_{\mu\nu}$ gives rise to couplings between the energy-momentum tensor $T_i^{\mu\nu}$ for all matter fields i and the graviton $h_{\mu\nu}$ as [26]

$$\sqrt{-g} \mathcal{L} \supset \frac{1}{M_P} h_{\mu\nu} \sum_i T_i^{\mu\nu}, \quad (2.7)$$

with $i = \{\phi, \chi, \text{SM}\}$. These gravitational interactions can play a crucial role in particle production in the early Universe, as we will discuss later.

3 Inflation and (P)reheating

In the following, we briefly review the dynamics of polynomial inflation and the cosmic (p)reheating taking place after inflation.

3.1 Polynomial Inflation

In polynomial inflation, the potential takes a form as given in Eq. (2.4). In the case where $b = \frac{9}{32} \frac{c^2}{d}$, the potential has an inflection point at $\phi = \phi_0 \equiv -\frac{3}{8} \frac{c}{d}$, and can be reparameterized as [18, 19]

$$V(\phi) = d \left[2\phi_0^2 \phi^2 - \frac{8}{3} (1 - \beta) \phi_0 \phi^3 + \phi^4 \right]. \quad (3.1)$$

The parameter β controls the flatness of the potential near ϕ_0 . For $\beta = 0$, one has an exact inflection point at ϕ_0 . A false vacuum is generated at $\phi > \phi_0$ if $\beta < 0$, in which case the inflaton may not roll down to the global minimum of the potential. The latter possibility,

¹A linear term can always be removed through a field redefinition.

²The results presented in this paper would be qualitatively similar for the case of a DM Majorana fermion. See Ref. [25] for a recent study of scalar DM production during reheating.

which is physically disfavored as it would not lead to a hot Big Bang, is avoided in this paper by only considering $0 < \beta \ll 1$.

We apply the SR approximation and define the following SR parameters [27]

$$\epsilon_V \equiv \frac{M_P^2}{2} \left(\frac{V'}{V} \right)^2, \quad \eta_V \equiv M_P^2 \frac{V''}{V}, \quad \xi_V^2 \equiv M_P^4 \frac{V' V'''}{V^2}, \quad (3.2)$$

which must be smaller than one during the accelerated expansion of the Universe. Inflation ends when the field reaches the value $\phi = \phi_{\text{end}}$ defined as $\epsilon_V(\phi_{\text{end}}) = 1$.³ The total number of e -folds N_\star between the time when the CMB pivot scale $k_\star = 0.05 \text{ Mpc}^{-1}$ first crossed the horizon until the end of inflation is given by [19]

$$\begin{aligned} N_\star &= \int_{\phi_{\text{end}}}^{\phi_\star} \frac{1}{\sqrt{2\epsilon_V(\phi)}} \frac{d\phi}{M_P} \\ &\simeq \frac{1}{24} \left[3 \left(\frac{\phi}{M_P} \right)^2 - 4 \frac{\phi \phi_0}{M_P^2} + 15 \left(\frac{\phi_0}{M_P} \right)^2 \right. \\ &\quad \left. - \left(\frac{\phi_0}{M_P} \right)^2 \sqrt{\frac{2}{\beta}} \arctan \left(\frac{\phi_0 - \phi}{\sqrt{2\beta} \phi_0} \right) - \left(\frac{\phi_0}{M_P} \right)^2 \ln \left(\frac{\phi_0 - \phi}{M_P} \right)^2 \right] \Big|_{\phi_{\text{end}}}^{\phi_\star}. \end{aligned} \quad (3.3)$$

In this work, we consider $50 \lesssim N_\star \lesssim 65$ [19, 28]. The power spectrum of the curvature perturbation \mathcal{P}_ζ , the spectral index n_s , its running α ,⁴ and the tensor-to-scalar ratio r are respectively given by [18, 19, 22]

$$\mathcal{P}_\zeta = \frac{1}{24\pi^2 \epsilon_V} \frac{V}{M_P^4}, \quad (3.4)$$

$$n_s = 1 - 6\epsilon_V + 2\eta_V, \quad (3.5)$$

$$\alpha = 16\epsilon_V \eta_V - 24\epsilon_V^2 - 2\xi_V^2, \quad (3.6)$$

$$r = 16\epsilon_V, \quad (3.7)$$

in the SR formalism. The observables are constrained by the Planck 2018 measurements including baryonic acoustic oscillations at the pivot scale $k_\star = 0.05 \text{ Mpc}^{-1}$ to [29]

$$\mathcal{P}_\zeta = (2.1 \pm 0.1) \times 10^{-9}, \quad n_s = 0.9659 \pm 0.0040, \quad \alpha = -0.0041 \pm 0.0067. \quad (3.8)$$

The most recent constraint on r is obtained from BICEP/Keck 2018 together with Planck data [30]:

$$r < 0.035, \quad \text{at 95\% C.L.} \quad (3.9)$$

Note that the model contains four parameters that play a role in inflation, namely d , β , ϕ_\star , and ϕ_0 . The value of ϕ_\star is fixed by setting the number of e -folds N_\star , while the three remaining degrees of freedom must satisfy the constraints in Eqs. (3.8) and (3.9). The parameter space allowed for ϕ_0 is found to be [18, 19]

$$3 \times 10^{-5} M_P \lesssim \phi_0 \lesssim 21.5 M_P. \quad (3.10)$$

³In large field inflation, the potential is dominated by the quadratic term at the end of inflation, which is independent of β .

⁴The running, defined as $\alpha \equiv \frac{dn_s}{d \ln k}$, describes the scale dependence of the spectral index.

For smaller ϕ_0 , it is required that ϕ_\star be close to ϕ_0 to fit the CMB data. In this case, even a small loop correction to the potential from the inflaton couplings could affect the flatness required by CMB observations [18]. On the other hand, for very large values of ϕ_0 , $\phi_\star \ll \phi_0$, the first term in Eq. (3.1) dominates. This implies that when ϕ_0 is larger than a critical value, the potential becomes near quadratic, $V(\phi) \simeq 2d\phi_0^2\phi^2$. The latter is in tension with the upper bound on r from BICEP/Keck 2018 data [30], which allows us to derive an upper bound on ϕ_0 .

Having presented the allowed range of ϕ_0 in Eq. (3.10), we can now discuss the parameter space of the inflaton mass m_ϕ , which is the second derivative of the potential in Eq. (3.1),

$$m_\phi = 2\sqrt{d}\phi_0 \simeq 5.14 \times 10^{-8} \left(\frac{\phi_0^2}{M_P} \right), \quad (3.11)$$

where the last equality was obtained by using $d \simeq 6.61 \times 10^{-16} (\phi_0/M_P)^2$.⁵ This analytical expression remains a good approximation for $\phi_0 \lesssim 5 M_P$. For $\phi_0 \gtrsim 5 M_P$, the range of d is found to be $10^{-13} \lesssim d \lesssim 10^{-14}$ [19]. From the constraints on d and ϕ_0 presented here and in Eq. (3.10), respectively, we find that the inflaton mass can acquire the following range of possible values

$$10^2 \text{ GeV} \lesssim m_\phi \lesssim 10^{13} \text{ GeV}. \quad (3.12)$$

Future CMB experiments could further constrain the upper limit on the inflaton mass. The prediction for the running α of the spectral index is negative and lies in the range [18, 19]

$$\alpha \in [-\mathcal{O}(10^{-2}), -\mathcal{O}(10^{-3})]. \quad (3.13)$$

In the left panel of Fig. 1, we show predictions in the $[n_s, r]$ plane for four benchmark scenarios for $50 \lesssim N_\star \lesssim 65$ indicated by a small and large red dot, respectively: $\phi_0 = 21.5 M_P$ and $\beta = 1 \times 10^{-3}$ (solid red), $\phi_0 = 11 M_P$ and $\beta = 19 \times 10^{-3}$ (red dashed), $\phi_0 = 8 M_P$ and $\beta = 6 \times 10^{-3}$ (dash-dotted red) and $\phi_0 = 5 M_P$ with $\beta = 10^{-3}$ (dotted red). Larger ϕ_0 corresponds to a higher inflationary scale with higher predictions for r . For fixed ϕ_0 , a larger β implies a steeper potential, giving rise to a larger prediction for r , as shown in the right panel of Fig. 1. The normalization d of the potential has no impact on these results. The blue shaded area indicates the parameter space allowed by the combination of BICEP/Keck 2018 and Planck data [30]. We note that future CMB experiments, such as CMB-S4 [31] could offer more stringent constraints on ϕ_0 , as shown in gray. As demonstrated above, polynomial inflation, depending on the parameters ϕ_0 , d , β , and ϕ_\star , can well accommodate recent CMB data. In the large-field scenario, the potential is dominated by the quadratic term when inflation ends, which is independent of β . For the focus of this paper, namely the DM production during reheating, the relevant parameters are the inflaton mass and the inflationary scale, which both depend on ϕ_0 .

3.2 (P)reheating

After the end of cosmic inflation, the inflaton oscillates around the minimum of its potential and transfers energy into a plasma of lighter degrees of freedom. The inflaton oscillates

⁵The parameter d controls the overall amplitude of the power spectrum \mathcal{P}_ζ and was obtained in Ref. [18] by fixing \mathcal{P}_ζ to the central value in Eq. (3.8).

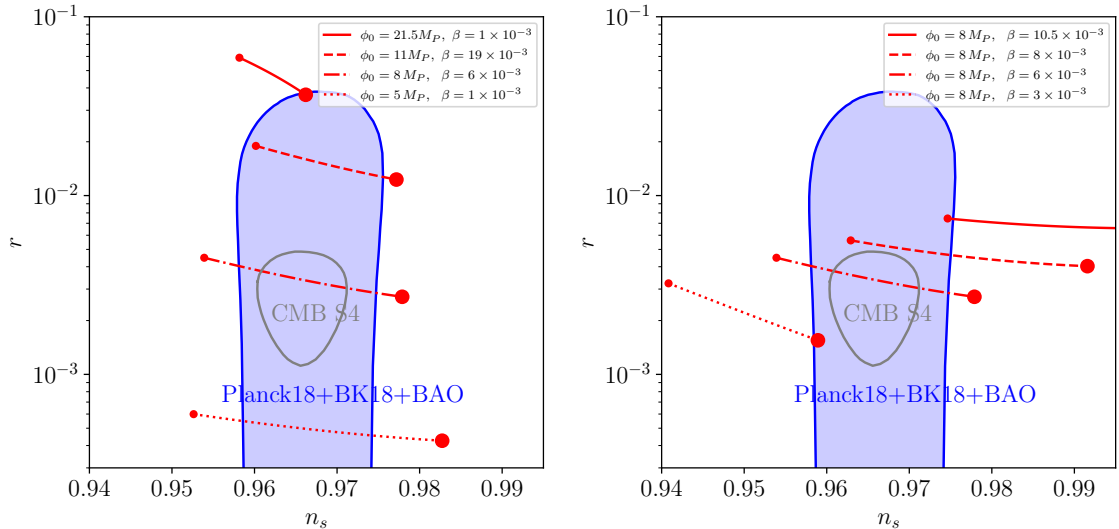


Figure 1. Left panel: Predictions in the $[n_s, r]$ plane for four benchmark values of ϕ_0 and fixed β . Right panel: Impact of β on inflationary predictions for fixed ϕ_0 . The small (large) red dot corresponds to $N_\star = 50$ ($N_\star = 65$). The blue shaded area is allowed by the combination of BICEP/Keck and Planck data [30], while the gray line corresponds to a projected sensitivity of CMB-S4 [31].

around $\phi = 0$ during reheating, where the quadratic term in Eq. (3.1) dominates, leading to $V(\phi) \simeq \frac{m_\phi^2}{2} \phi^2$. In our setup, the dominant channel for energy transfer is the decay of inflatons into pairs of SM Higgs bosons with mass m_H . The corresponding decay rate reads

$$\Gamma_\phi = \frac{1}{8\pi} \frac{\mu^2}{m_\phi} \left[1 - \left(\frac{2m_H}{m_\phi} \right)^2 \right]^{1/2}. \quad (3.14)$$

The evolution of the inflaton energy density, ρ_ϕ , and the radiation energy density, ρ_R , are governed by the following set of Boltzmann equations

$$\frac{d\rho_\phi}{dt} + 3\mathcal{H}\rho_\phi = -\Gamma_\phi\rho_\phi, \quad (3.15)$$

$$\frac{d\rho_R}{dt} + 4\mathcal{H}\rho_R = +\Gamma_\phi\rho_\phi, \quad (3.16)$$

where the Hubble expansion rate \mathcal{H} is determined from the Friedmann equation

$$\mathcal{H}^2 = \frac{\rho_R + \rho_\phi}{3M_P^2}. \quad (3.17)$$

An approximate analytical solution for the SM energy density during reheating is

$$\rho_\phi(a) \simeq \rho_\phi(a_{\text{end}}) \left(\frac{a_{\text{end}}}{a} \right)^3, \quad (3.18)$$

which is valid as long as $\mathcal{H} \gg \Gamma_\phi$. Here, a_{end} corresponds to the scale factor at the end of inflation and the beginning of reheating, $\rho_R(a_{\text{end}}) = 0$ and $\rho_\phi(a_{\text{end}}) = 3M_P^2\mathcal{H}^2(a_{\text{end}})$.

The inflationary Hubble scale $\mathcal{H}(a_{\text{end}})$ is given by the Friedmann equation $\mathcal{H}^2(a_{\text{end}}) \simeq V(a_{\text{end}})/(3M_P^2)$. Using Eq. (3.18), the solution for ρ_R during reheating takes the form

$$\rho_R(a) = \frac{6}{5} M_P^2 \Gamma_\phi \mathcal{H}(a_{\text{end}}) \left(\frac{a_{\text{end}}}{a}\right)^{\frac{3}{2}} \left[1 - \left(\frac{a_{\text{end}}}{a}\right)^{\frac{5}{2}}\right]. \quad (3.19)$$

While we have verified the validity of the above analytical approximations, we obtain our numerical results by solving the full set of Boltzmann equations without relying on any approximations.

The SM radiation energy density is defined as a function of the temperature T of the SM bath as⁶

$$\rho_R(T) = \frac{\pi^2}{30} g_\star(T) T^4, \quad (3.20)$$

where $g_\star(T)$ corresponds to the number of relativistic degrees of freedom contributing to the SM energy density. The end of reheating is determined by the onset of SM radiation domination, at a temperature $T = T_{\text{rh}}$. We define the reheating temperature by the equality $\mathcal{H}(T_{\text{rh}}) \equiv \frac{2}{3}\Gamma_\phi$, assuming that the inflaton decays away at a time scale $t = 1/\Gamma_\phi$,

$$T_{\text{rh}}^2 = \frac{2}{\pi} \left(\frac{10}{g_\star(T_{\text{rh}})}\right)^{\frac{1}{2}} M_P \Gamma_\phi. \quad (3.21)$$

We require $T_{\text{rh}} > T_{\text{BBN}} \simeq 4$ MeV to leave the standard BBN predictions unaffected by our setup [37–41]. Furthermore, the SM energy density in Eq. (3.19) has a maximum at $a = a_{\text{max}} \equiv (8/3)^{2/5} a_{\text{end}}$, and the corresponding maximum temperature T_{max} [42] is given by

$$T_{\text{max}}^4 = \frac{60}{\pi^2 g_\star(T_{\text{max}})} \left(\frac{3}{8}\right)^{\frac{8}{5}} M_P^2 \Gamma_\phi \mathcal{H}(a_{\text{end}}), \quad (3.22)$$

which is an important parameter in the UV freeze-in process to be discussed in the next section. Finally, considering that during reheating the temperature scales as $T(a) \propto a^{-3/8}$ (cf. Eq. (3.19)), it follows that the Hubble expansion rate can be expressed as

$$\mathcal{H}(T) = \frac{\pi}{3} \frac{T^2}{M_P} \times \begin{cases} \sqrt{\frac{g_\star(T_{\text{rh}})}{10}} \left(\frac{T}{T_{\text{rh}}}\right)^2 & \text{for } T_{\text{max}} > T \geq T_{\text{rh}}, \\ \sqrt{\frac{g_\star(T)}{10}} & \text{for } T_{\text{rh}} \geq T. \end{cases} \quad (3.23)$$

This result will later be used to analytically solve the Boltzmann equation governing DM production.

To illustrate the preceding discussion, in Fig. 2 we depict the evolution of the radiation and inflaton energy densities (left) and the SM temperature (right), for the largest possible value $\phi_0 = 21.5 M_P$ and $m_\phi \simeq 1.5 \times 10^{13}$ GeV (the latter is obtained from Eq. (3.11))

⁶As the produced particles interact with the plasma, they eventually thermalize [32, 33]. In this work, we assume that the thermalization process occurs instantaneously, which is a good approximation if the reheating process is not dominated by Planck-suppressed operators [34]. If the instantaneous-thermalization assumption is violated, then the decay products could follow initial distributions with lower occupation numbers and harder momenta [34–36].

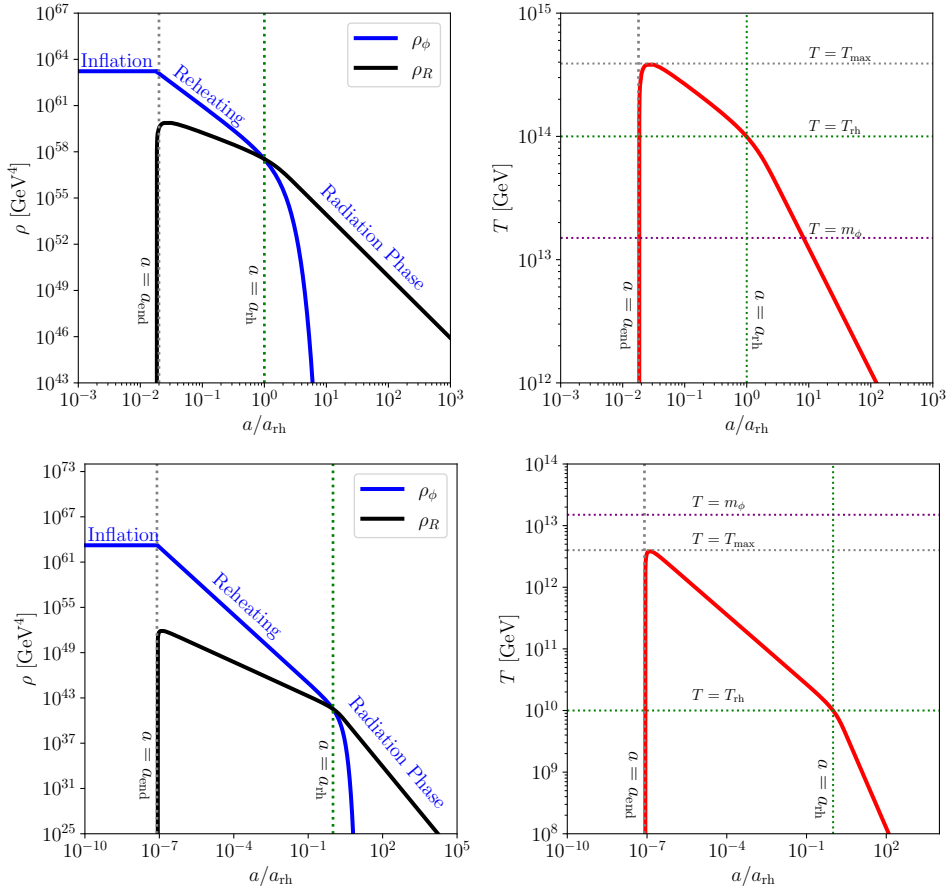


Figure 2. Evolution of energy densities (left) and SM temperature (right) for $T_{\text{rh}} = 10^{14}$ GeV (top) and $T_{\text{rh}} = 10^{10}$ GeV (bottom) with for $\phi_0 = 21.5 M_P$ and $m_\phi \simeq 1.5 \times 10^{13}$ GeV.

using $d \simeq 2 \times 10^{-14}$). We have numerically solved the coupled Boltzmann equations (3.15) and (3.16) for two scenarios $T_{\text{rh}} = 10^{14}$ GeV (upper panel) and $T_{\text{rh}} = 10^{10}$ GeV (lower panel). The former value is the largest possible reheating temperature allowed in the large field inflation scenario as we will see in the following, and the latter illustrates a scenario featuring a reheating temperature lower than the inflaton mass. In a bosonic reheating process, it is possible to reach temperatures higher than the inflaton mass due to soft bosons rescattering and forming harder degrees of freedom [18]. For fixed reheating temperature, the inflaton decay rate appearing in the Boltzmann equation is obtained via $\Gamma_\phi = 3/2\mathcal{H}(T_{\text{rh}})$ with $\mathcal{H}(T_{\text{rh}}) = \frac{\pi}{3} \sqrt{\frac{g_\star(T_{\text{rh}})}{10}} \frac{T_{\text{rh}}^2}{M_P}$. The inflaton does not thermalize during reheating even though the temperature can be larger than the inflaton mass, since the temperature-independent inflaton interaction rate Γ_ϕ is always smaller than the Hubble rate during reheating. Given its relevance to the discussion of the DM production, we emphasize that during reheating, the maximum temperature T_{max} can be much higher than T_{rh} [42], as shown in the lower right panel of Fig. 2.

In general, inflaton couplings to other particles could spoil the flatness of the potential during inflation. In the polynomial inflationary setup, the radiative stability of the infla-

ton potential during inflation requires a suppressed inflaton-Higgs coupling, which in turn requires [18]

$$\left| \left(\frac{\mu}{\phi_0} \right)^2 \ln \left(\frac{\mu}{\phi_0} \right) - \left(\frac{\mu}{\phi_0} \right)^2 \right| < 64\pi^2 d\beta, \quad (3.24)$$

and translates into an upper bound on the coupling μ . The constraint on μ shown in Eq. (3.24) together with the upper bound on $\phi_0 = 21.5M_P$ in Eq. (3.10) gives rise to an upper bound on the maximal reheating temperature [19]

$$T_{\text{rh}} \lesssim 10^{14} \text{ GeV}. \quad (3.25)$$

We emphasize that the upper bound on T_{rh} depends on ϕ_0 and the couplings involved for the reheating. For smaller ϕ_0 , e.g. $\phi_0 = M_P$, it has been shown that $T_{\text{rh}} \lesssim 10^{11} \text{ GeV}$ [18]. Similarly, DM would also contribute (negatively) to the inflaton potential at loop level, which could potentially spoil inflationary predictions. To keep radiative corrections under control, y_χ must satisfy [18]

$$|y_\chi^4 - 3y_\chi^4 \ln(y_\chi^2)| < 64\pi^2 d\beta. \quad (3.26)$$

Assuming the upper bound on $\phi_0 = 21.5M_P$ and taking into account the allowed range of d and β within the 2σ range of the BICEP 2018 data, we obtain

$$y_\chi \lesssim 10^{-4}. \quad (3.27)$$

We note that within our framework, non-perturbative preheating and pure gravitational reheating are subdominant to perturbative decay. The trilinear coupling, $\mu\phi|H|^2$, which induces a tachyonic squared-mass $m_H^2 \sim \mu\phi$ for the field H once ϕ becomes negative after crossing zero, tends to make preheating efficient. However, the quartic self-interaction term, $\lambda_H H^4$, introduces a positive squared mass term $m_H^2 \sim \lambda_H \langle H^2 \rangle$, where $\langle H^2 \rangle$ denotes the variance of H . This backreaction effectively counteracts the tachyonic effects, quickly terminating preheating and rendering it inefficient [43]. Finally, we comment on the possibility of gravitational reheating. It has been established that rather steep inflaton potentials $V \sim \phi^p$ with $p > 9$ are required at the reheating stage for successful gravitational reheating [44–47]. Interestingly, this bound can be relaxed to $p > 4$ by introducing a non-minimal coupling between gravity and two inflatons [48], or even to $p \geq 2$ by coupling gravity non-minimally to a single inflaton [49]. In our case, the inflaton oscillates around a quadratic potential $V(\phi) \propto \frac{1}{2} m_\phi^2 \phi^2$ during reheating and is minimally coupled to gravity, making gravitational reheating inefficient. It is therefore ignored in the following.

4 Dark Matter Production

In the following, we aim to quantify DM production within the large-field inflationary model during and after reheating. The evolution of the DM number density n can be tracked using the Boltzmann equation

$$\frac{dn}{dt} + 3\mathcal{H}n = \gamma, \quad (4.1)$$

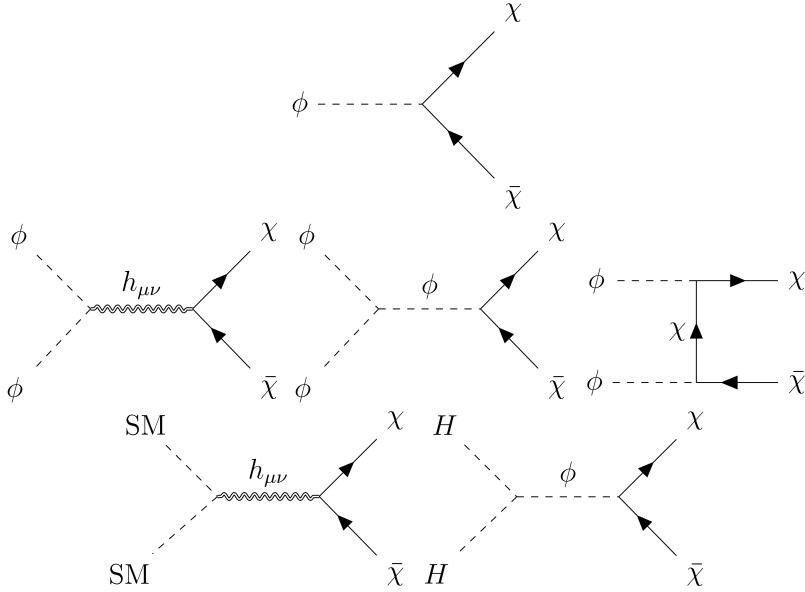


Figure 3. Feynman diagram for fermionic DM production.

where γ denotes the DM production rate density. Taking into account that during reheating the SM entropy is not conserved, it is convenient to introduce a comoving number density $N \equiv n a^3$, with which the Boltzmann Eq. (4.1) can be rewritten as

$$\frac{dN}{da} = \frac{a^2 \gamma}{\mathcal{H}}, \quad (4.2)$$

or equivalently as

$$\frac{dN}{dT} = \begin{cases} -\frac{8}{\pi} \sqrt{\frac{10}{g_*(T_{\text{rh}})}} \frac{M_P T_{\text{rh}}^{10}}{T^{13}} a^3(T_{\text{rh}}) \gamma & \text{for } T_{\text{max}} > T \geq T_{\text{rh}}, \\ -\frac{3}{\pi} \sqrt{\frac{10}{g_*(T)}} \frac{g_{*s}(T_{\text{rh}})}{g_{*s}(T)} \frac{M_P T_{\text{rh}}^3}{T^6} a^3(T_{\text{rh}}) \gamma & \text{for } T_{\text{rh}} \geq T, \end{cases} \quad (4.3)$$

using Eq. (3.23). We solve Eq. (4.3) to obtain the number density. To facilitate a comparison with observational data, we introduce the DM yield $Y(T) \equiv n(T)/s(T)$ as a function of the SM entropy density $s(T) \equiv \frac{2\pi^2}{45} g_{*s}(T) T^3$, where $g_{*s}(T)$ is the number of relativistic degrees of freedom that contribute to the SM entropy. To fit the observed relic abundance, the DM yield has been fixed such that

$$m_\chi Y_0 = \Omega_\chi h^2 \frac{1}{s_0} \frac{\rho_c}{h^2} \simeq 4.3 \times 10^{-10} \text{ GeV}, \quad (4.4)$$

with $\rho_c \simeq 1.05 \times 10^{-5} h^2 \text{ GeV/cm}^3$ the critical energy density of the Universe, $s_0 \simeq 2.9 \times 10^3 \text{ cm}^{-3}$ the present entropy density [50], and $\Omega_\chi h^2 \simeq 0.12$ [29].

The relevant tree-level processes that contribute to DM production are depicted in Fig. 3, and include

- Inflaton decay (first row),
- Inflaton scattering (second row),
- SM particle scattering (third row),

which we will investigate in the following three subsections, respectively.

4.1 Inflaton Decay

The interaction rate density associated with the production of pairs of DM particles from inflaton decays (through the trilinear interaction in Eq. (2.5)) is given by

$$\gamma = 2 n_\phi \Gamma_\phi \text{Br}, \quad (4.5)$$

where $n_\phi = \rho_\phi/m_\phi$ denotes the inflaton number density, and Γ_ϕ is given in Eq. (3.14). Note that two DM particles are produced in each inflaton decay, which is accounted for by the factor 2 in Eq. (4.5). Additionally, the branching ratio, Br, for the decay of the inflaton into DM is given by

$$\text{Br} \equiv \frac{\Gamma_{\phi \rightarrow \bar{\chi}\chi}}{\Gamma_{\phi \rightarrow H^\dagger H} + \Gamma_{\phi \rightarrow \bar{\chi}\chi}} \simeq y_\chi^2 \left(\frac{m_\phi}{\mu} \right)^2 \left(1 - \frac{4m_\chi^2}{m_\phi^2} \right)^{3/2}, \quad (4.6)$$

where we have neglected the Higgs mass. With the interaction rate in Eq. (4.5), one can solve Eq. (4.3) during reheating, i.e. for $T_{\text{max}} \geq T \geq T_{\text{rh}}$, and obtain

$$N(a_{\text{rh}}) \equiv N(T_{\text{rh}}) \simeq \frac{2\pi g_*(T_{\text{rh}})}{15} \sqrt{\frac{10}{g_*(T_{\text{rh}})}} \text{Br} \frac{M_P T_{\text{rh}}^2 \Gamma_\phi}{m_\phi} a_{\text{rh}}^3, \quad (4.7)$$

from which we arrive at the DM yield at present

$$Y_0 = Y_{\text{rh}} = \frac{N(a_{\text{rh}})}{s(T_{\text{rh}}) a_{\text{rh}}^3} \simeq \frac{3}{2} \frac{g_*(T_{\text{rh}})}{g_{*s}(T_{\text{rh}})} \frac{T_{\text{rh}}}{m_\phi} \text{Br} \simeq \frac{3 y_\chi^2}{8\pi^2} \frac{\sqrt{10 g_*(T_{\text{rh}})}}{g_{*s}(T_{\text{rh}})} \frac{M_P}{T_{\text{rh}}}. \quad (4.8)$$

Note that DM production from inflaton decay is exponentially suppressed after reheating and can be neglected.

In Fig. 4, we show with thick black lines the parameter space $[m_\chi, T_{\text{rh}}]$ required to reproduce the observed DM relic density through inflaton decays, for several benchmark values for the Yukawa coupling y_χ . As an example, we have again fixed $\phi_0 = 21.5 M_P$, which corresponds to an inflaton mass $m_\phi \simeq 1.5 \times 10^{13}$ GeV for $d = 2 \times 10^{-14}$. Energy conservation dictates that only DM with masses up to $m_\phi/2$ can be produced from inflaton decays, as illustrated by the vertical red line in Fig. 4. Several constraints to the model parameters are overlaid in color. Low reheating temperatures with $T_{\text{rh}} \lesssim 4$ MeV [37–41] are in tension with BBN, whereas high reheating temperatures and large Yukawa couplings are disfavored due to the destabilization of the inflaton potential when including loop corrections, cf. Eqs. (3.25) and (3.27). Finally, small masses are not allowed due to the Lyman- α constraints: The DM particles produced from inflaton decays had an initial

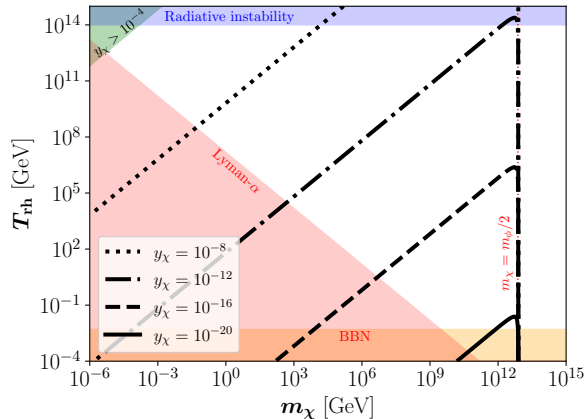


Figure 4. Parameter space that reproduces the observed DM abundance for DM produced through 2-body decays of the inflaton for different values of the Yukawa coupling y_χ with $m_\phi = 1.5 \times 10^{13}$ GeV and $\phi_0 = 21.5 M_P$ (thick black lines). The colored bands are in tension with BBN (orange), Lyman- α (red) or generate radiative corrections from Higgs (blue) or DM loops (green) to the potential that could spoil the flatness required for successful inflation. The vertical red dotted line corresponds to $m_\chi = m_\phi/2$.

energy $E_\chi = m_\phi/2$ at the time of production. Due to redshifting, the present momentum of the DM particles is $p_\chi(a_0) = E_\chi \times a_{\text{rh}}/a_0$ with a_0 and a_{rh} being the scale factors at present and at the end of reheating, respectively. As a cold DM candidate, it is required that the DM velocity at present is smaller than that of warm DM constrained by Lyman- α , namely $p_\chi(a_0)/m_\chi \lesssim 1.8 \times 10^{-8}$ [51], which leads to [22]

$$\frac{m_\chi}{\text{keV}} \gtrsim \frac{m_\phi}{T_{\text{rh}}}. \quad (4.9)$$

The Lyman- α constraint and the condition $y_\chi < 10^{-4}$ can be combined to give a lower bound on the DM mass

$$m_\chi \gtrsim 4.8 \text{ keV}. \quad (4.10)$$

We note that compared to the previous analysis in a small-field model [22], where $m_\chi \lesssim 10^{11}$ GeV, DM can be as large as $m_\chi \simeq m_\phi/2 \sim 10^{13}$ GeV in the large-field scenario. However, other production channels, e.g. gravitational production, can also be efficient in the large-field scenario and will modify the results presented in Fig. 4, as we demonstrate below.

4.2 Inflaton Scattering

In addition to the production from inflaton decays, DM particles are also generated from inflaton scatterings, as shown in the second row of Fig. 3. The relevant processes are s -channel annihilations mediated by a graviton or an inflaton (due to the ϕ^3 term in the potential) and t -channel annihilations mediated by DM. Compared to decays, the inflaton-mediated s -channel and DM-mediated t -channel annihilations are always suppressed because of extra couplings appearing in the cross section. We thus only focus on gravitational annihilation,

which dominates the production if the direct coupling between the inflaton and the DM is sufficiently suppressed.

For the DM production from gravitational annihilation of inflatons, the interaction-rate density is given by [52–55]

$$\gamma = \frac{\rho_\phi^2}{m_\phi^2} \frac{m_\chi^2}{64\pi M_P^4} \left(1 - \frac{m_\chi^2}{m_\phi^2}\right)^{3/2}, \quad (4.11)$$

where m_χ in the second term arises from spin summation in the final states. A detailed derivation of Eq. (4.11) can be found in appendix A. The corresponding DM yield at present is

$$Y_0 \simeq \frac{g_\star}{128 g_{\star s}} \sqrt{\frac{g_\star}{10}} \left(\frac{m_\chi}{m_\phi}\right)^2 \left(\frac{T_{\text{rh}}}{M_P}\right)^3 \left[\left(\frac{T_{\text{max}}}{T_{\text{rh}}}\right)^4 - 1\right] \left(1 - \frac{m_\chi^2}{m_\phi^2}\right)^{3/2}. \quad (4.12)$$

Note that the enhancement factor $[(T_{\text{max}}/T_{\text{rh}})^4 - 1]$ arises from the noninstantaneous nature of reheating. In large field polynomial inflation, a large ratio $T_{\text{max}}/T_{\text{rh}}$ naturally occurs (cf. Fig. 2), and the corresponding large enhancement of gravitational DM production from inflaton annihilation can successfully account for the observed relic abundance, as depicted by the solid black line in Fig. 5. For inflaton masses of the order $m_\phi \sim 10^{13}$ GeV, gravitational production is efficient even when the reheating temperature is as low as $T_{\text{rh}} \sim 10^5$ GeV in the regime where the mass of the DM reaches its kinematic threshold. Note that when $m_\chi = m_\phi$, the production is closed from the phase space. By comparing Eq. (4.12) and Eq. (4.8), we find that for a given reheating temperature T_{rh} , inflaton mass m_ϕ , and DM mass $m_\chi (\lesssim m_\phi/2)$, the gravitational annihilation dominates over the decay if

$$y_\chi \lesssim \frac{\pi}{4} \sqrt{\frac{g_\star}{30}} \frac{m_\chi}{m_\phi} \left(\frac{T_{\text{max}}}{M_P}\right)^2. \quad (4.13)$$

So far we have focused on production channels for DM with mass $m_\chi \lesssim m_\phi$. As mentioned previously, the temperature during reheating in the large-field scenario can be larger than the inflaton mass. This means that it is possible to source DM with a mass as large as T_{max} through the scattering of SM particles from the plasma, as we demonstrate in the next section.

4.3 SM Particles Scattering

In the following, we explore the DM production from scatterings of SM particles (last row of Fig. 3), mediated by either the graviton or inflaton. These processes allow the production of DM with $m_\chi \sim T_{\text{max}}$ and feature a UV freeze-in behavior due to the suppression of a heavy scale.

4.3.1 Graviton Mediation

For gravitational DM production from the annihilation of SM particles in the thermal plasma, the interaction rate is given by [56–59]

$$\gamma \simeq \alpha_f \frac{T^8}{M_P^4}, \quad (4.14)$$

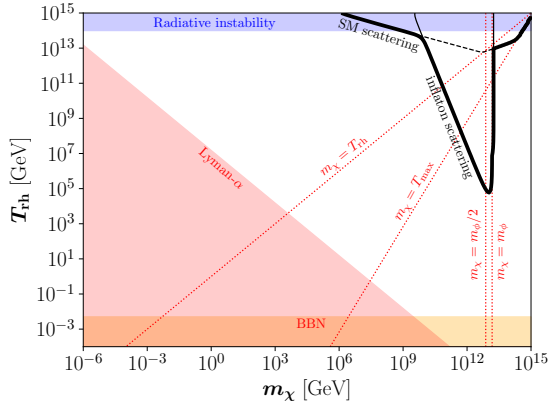


Figure 5. Parameter space that reproduces the observed DM abundance for DM produced through gravitational scatterings of inflatons or SM particles with $m_\phi = 1.5 \times 10^{13}$ GeV and $\phi_0 = 21.5 M_P$ (thick black lines). The colored bands are in tension with BBN (orange), Lyman- α (red) or generate a radiative-unstable potential (blue). The vertical red dotted lines correspond to $m_\chi = m_\phi/2$, $m_\chi = m_\phi$, $m_\chi = T_{\text{rh}}$ and $m_\chi = T_{\text{max}}$.

where $\alpha_f \simeq 1.1 \times 10^{-3}$ is obtained for fermionic DM by summing over the contributions from all SM degrees of freedom in the thermal plasma [58]. The corresponding DM yield at present is given by

$$Y_0 \simeq \begin{cases} \frac{45 \alpha_f}{2\pi^3 g_{*s}} \sqrt{\frac{10}{g_*}} \frac{T_{\text{rh}}^3}{M_P^3} \left\{ \left[1 - \left(\frac{m_\chi}{T_{\text{rh}}} \right)^3 \right] + 2 \left[1 - \left(\frac{T_{\text{rh}}}{T_{\text{max}}} \right)^4 \right] \right\} \simeq \frac{135 \alpha_f}{2\pi^3 g_{*s}} \sqrt{\frac{10}{g_*}} \frac{T_{\text{rh}}^3}{M_P^3} & \text{for } m_\chi \lesssim T_{\text{rh}}, \\ \frac{45 \alpha_f}{\pi^3 g_{*s}} \sqrt{\frac{10}{g_*}} \frac{T_{\text{rh}}^7}{M_P^3 m_\chi^4} \left[1 - \left(\frac{m_\chi}{T_{\text{max}}} \right)^4 \right] & \text{for } T_{\text{rh}} \lesssim m_\chi \lesssim T_{\text{max}}. \end{cases} \quad (4.15)$$

DM lighter than T_{rh} is produced both during and after reheating, while DM heavier than T_{rh} (and lighter than T_{max}) is produced only during reheating. For $m_\chi \lesssim T_{\text{rh}}$, the gravitational scattering of SM particles is subdominant compared to the channels studied in the two preceding subsections. However, in contrast to the channels considered in Sections 4.1 and 4.2, gravitational scattering of SM particles can account for the observed relic abundance even if $m_\chi \gtrsim m_\phi$, as shown by the solid black line in the upper right corner of Fig. 5. Consequently, DM as heavy as $m_\chi \simeq T_{\text{max}} \simeq 4 \times 10^{14}$ GeV can be produced in the large-field polynomial inflation scenario, which is three orders of magnitude larger than the upper limit in the small-field scenario.

4.3.2 Inflaton Mediation

Finally, we focus on the inflaton-mediated UV freeze-in production of DM from scatterings of SM particles, as depicted in the second diagram of the last row of Fig. 3. The annihilation

cross section σ for this process is given by

$$\sigma(\mathfrak{s}) \simeq \frac{1}{8\pi} \frac{y_\chi^2 \mu^2}{(\mathfrak{s} - m_\phi^2)^2 + m_\phi^2 \Gamma_\phi^2} \left(1 - \frac{4m_\chi^2}{\mathfrak{s}}\right)^{3/2}, \quad (4.16)$$

where $\sqrt{\mathfrak{s}}$ corresponds to the center-of-mass energy.⁷ Since the SM temperature can be higher than the inflaton mass, the DM can be produced resonantly during reheating [61]. The corresponding interaction rate density is

$$\gamma(T) \simeq \frac{T}{8\pi^4} \int_{4m_\chi^2}^{\infty} d\mathfrak{s} \mathfrak{s}^{3/2} \sigma(\mathfrak{s}) K_1\left(\frac{\sqrt{\mathfrak{s}}}{T}\right), \quad (4.17)$$

and is well approximated by [62, 63]

$$\gamma(T) \simeq \frac{y_\chi^2 \mu^2}{64\pi^4} \times \begin{cases} \frac{32}{\pi} \frac{T^6}{m_\phi^4} & \text{for } T \ll m_\phi, \\ \frac{m_\phi^2 T}{\Gamma_\phi} K_1\left(\frac{m_\phi}{T}\right) \left[1 - \left(\frac{2m_\chi}{m_\phi}\right)^2\right]^{3/2} & \text{for } T \gtrsim m_\phi, \end{cases} \quad (4.18)$$

where K_1 denotes the modified Bessel function of the first kind. The analytical approximations shown in Eq. (4.18) have been validated against the full numerical result. Finally, as a consistency check, we note that DM does not thermalize, as $\gamma(T) \ll \mathcal{H}(T) n_{\text{eq}}(T)$ with $n_{\text{eq}}(T) \simeq \frac{4}{\pi^2} T^3$ for $T \gg m_\chi$.

The inflaton mass is typically larger than the reheating temperature due to the radiative stability condition [18, 22]. In the case where $m_\phi \gg T_{\text{rh}}$, which almost always holds for small-field inflation and sometimes also for large-field inflation, we obtain the following analytic approximation for the DM yield produced from inflaton-mediated Higgs decays using the first line of Eq. (4.18),⁸

$$Y_0 \simeq \frac{195 y_\chi^2}{4\pi^8 g_{\star s}} \sqrt{\frac{10}{g_\star}} \frac{\mu^2 T_{\text{rh}} M_P}{m_\phi^4} \simeq \frac{195 y_\chi^2}{g_{\star s} \pi^6} \left(\frac{T_{\text{rh}}}{m_\phi}\right)^3. \quad (4.19)$$

This result is parametrically suppressed by a factor

$$\frac{T_{\text{rh}}}{M_P} \left(\frac{T_{\text{rh}}}{m_\phi}\right)^3 \ll 1 \quad (4.20)$$

compared to the contribution from inflaton decays (cf. Eq. (4.8)), and hence always negligible.

However, in large-field scenarios, it is also possible to have $T_{\text{rh}} \gtrsim m_\phi$. In this case, we find that the ratio of the DM yield between annihilation and decay is proportional to a factor $T_{\text{rh}}/(g_\star m_\phi)$. This result is obtained by solving Eq. (4.3) using the analytical

⁷We take the Higgs to be massless before the onset of the electroweak phase transition. The thermal mass of the Higgs is dominated by $\sim \frac{1}{4} y_t T$ with y_t being the quark-top Yukawa coupling [60], which is negligible compared to the momentum of the thermal Higgs.

⁸Equation (4.19) refines the result reported in Ref. [22] by a factor 195/135 accounting for the DM production during reheating, which was not considered previously.

expressions in Eq. (4.18).⁹ Numerically, we find that in the most extreme case of large-field polynomial inflation consistent with CMB data, where $T_{\text{rh}} \sim 10^{14}$ GeV, inflaton-mediated Higgs annihilation provides a percent level correction to the DM relic abundance produced from inflaton decays.

4.4 Combined analysis

In the following, we combine *all* previously studied processes and investigate their interplay for different DM masses m_χ and reheating temperatures T_{rh} . Figure 6 shows, with thick black lines, the parameter space that reproduces the entire observed DM abundance considering all processes previously discussed. From left to right, we show the results for different values of the Yukawa coupling y_χ with $\phi_0 = 21.5 M_P$ (first column), $\phi_0 = 5 M_P$ (second column) and $\phi_0 = 0.8 M_P$ (third column). The two red dotted vertical lines correspond to $m_\chi = m_\phi$ and $m_\chi = m_\phi/2$.

We start by considering the largest possible value $\phi_0 = 21.5 M_P$, corresponding to $m_\phi = 1.5 \times 10^{13}$ GeV, shown in the four panels to the left. The upper panel shows the viable parameter space for $y_\chi = 10^{-8}$, and the lower panels show how the parameter space changes as the value of y_χ is lowered. For y_χ larger than a threshold value, the viable parameter space is continuous in T_{rh} and discontinuous in m_χ , as seen in the three upper panels. As y_χ is lowered below a threshold value, the parameter space becomes continuous in m_χ and discontinuous in T_{rh} . We find numerically that the threshold value is $y_\chi \approx 10^{-17}$, which is in agreement with the analytical threshold value obtained in Eq. (4.13). For $y_\chi \gtrsim 10^{-17}$, the branch to the left corresponds to light DM ($m_\chi < m_\phi/2$), which is produced via both inflaton decays and graviton-mediated annihilations of inflatons and SM particles. The branch to the right corresponds to heavier DM masses ($m_\phi/2 \lesssim m_\chi < T_{\text{max}}$) and is independent of the value of the Yukawa coupling y_χ for $T_{\text{rh}} \gtrsim 10^5$ GeV, where DM production is dominated by gravitational processes.¹⁰ DM is overproduced between the two branches, while it is underproduced in the two complementary regions of parameter space. For $y_\chi \lesssim 10^{-17}$, there is a continuous range of viable DM masses that could account for the whole observed relic abundance, 10^9 GeV $\lesssim m_\chi < T_{\text{max}}$, where both upper and lower limits come from the intersection of gravitational production from scattering of SM particles and the constraint from radiative stability. Here, two branches occur for different values of T_{rh} : If $T_{\text{rh}} \gtrsim 10^5$ GeV, DM is produced by gravitational processes, whereas if $T_{\text{rh}} \lesssim 10^5$ GeV it is generated by the decay of the inflaton. Note that the black lines correspond to the parameter space where the correct relic abundance is reached, while the white region within them corresponds to overproduction. The remaining part leads to underproduction.

As ϕ_0 decreases, the maximum allowed value for the reheating temperature T_{rh} decreases, resulting in suppression of the gravitational production channels. Consequently, the interplay between graviton-mediated processes and inflaton decay becomes less promi-

⁹Obtaining a full analytical result for the yield Y_0 , analogous to Eq. (4.19), is considerably more complex for the present case due to the different scales involved, hence we do not present a corresponding result.

¹⁰For $T_{\text{rh}} \lesssim 10^5$ GeV, and DM masses very close to the kinematic threshold, DM production is dominated by inflaton decays.

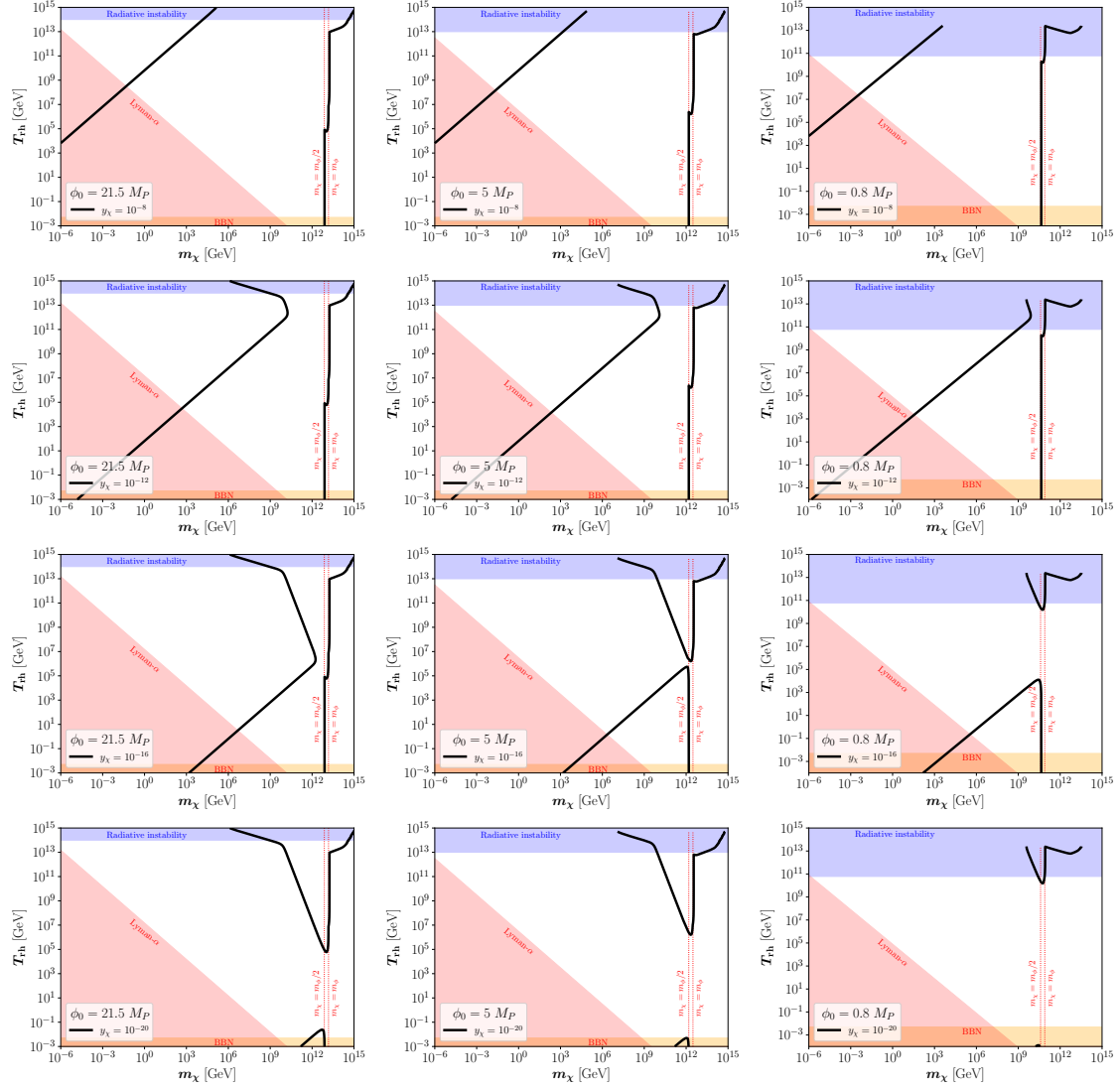


Figure 6. Parameter space (thick black lines) that reproduce the whole observed DM abundance taking into account *all* processes discussed in the text, for different values of the Yukawa coupling y_χ and $\phi_0 = 21.5 M_P$ (first column), $\phi_0 = 5 M_P$ (second column) and $\phi_0 = 0.8 M_P$ (third column). The colored bands are in tension with BBN (orange), Lyman- α (red) or generate a radiative-unstable potential (blue). The two red dotted vertical lines correspond to $m_\chi = m_\phi$ and $m_\chi = m_\phi/2$.

ment and eventually vanishes for smaller values of ϕ_0 , as shown in the second and third columns of Figure 6. In practice, we find that for $m_\phi \lesssim 10^{11}$ GeV or equivalently $\phi_0 \lesssim 0.8 M_P$, gravitational channels can no longer account for the DM relic abundance in any part of the parameter space that is consistent with the radiative bound on T_{rh} , as seen in the third column of Fig. 6.

5 Conclusions

Polynomial inflation is a simple cosmological framework that is consistent with the cosmic microwave background data and provides testable predictions for the tensor-to-scalar ratio and the running of the spectral index [18, 19]. However, it is desirable that a consistent cosmological model also explains other observations, including the dark matter (DM) abundance. Within the polynomial inflation framework, it was shown in Ref. [22] that for small field values, the direct decay of the inflaton dominates over all other production mechanisms due to the upper bound on the reheating temperature. However, the maximum reheating temperature can be up to three orders of magnitude higher in large-field scenarios compared to the small-field case. Consequently, DM-production channels that are suppressed in the small-field setup become important in the large-field setup.

We investigated all relevant production channels, including inflaton decays and inflaton- and graviton-mediated scatterings; see Fig. 3 for the relevant Feynman diagrams. We find that gravitational inflaton annihilations dominate over inflaton decays, for inflaton-DM couplings smaller than the threshold value presented in Eq. (4.13). When considering all production channels simultaneously, the parameter space (m_χ, T_{rh}) where the whole DM relic abundance is correctly accounted for is generally separated into two disconnected branches. For y_χ larger than a threshold value, the two branches are separated by a range of values for m_χ where the correct relic abundance cannot be accounted for. For y_χ smaller than the threshold, the two branches are separated by a range of values for T_{rh} where the relic abundance cannot be correctly reproduced, see Fig. 6 for details. Finally, we find that graviton-mediated SM particle annihilation can account for the whole relic abundance for DM masses as heavy as the maximum temperature $T_{\text{max}} \sim 10^{14}$ GeV, which is three orders of magnitude higher than the heaviest DM mass that can be accommodated in the small field setup.

In summary, the current work offers a comprehensive investigation of DM production after large-field polynomial inflation. The presented formalism can be readily extended to other inflationary setups.

Acknowledgments

NB received funding from the Spanish FEDER / MCIU-AEI under the grant FPA2017-84543-P. MAM acknowledges support from the DFG Collaborative Research Centre “Neutrinos and Dark Matter in Astro- and Particle Physics” (SFB 1258). JH, MAM, and YX acknowledge support from the Cluster of Excellence “Precision Physics, Fundamental Interactions, and Structure of Matter” (PRISMA⁺ EXC 2118/1) funded by the Deutsche Forschungsgemeinschaft (DFG, German Research Foundation) within the German Excellence Strategy (Project No. 390831469).

A Gravitational Scattering

In this appendix, we present a detailed derivation of the interaction-rate density for DM production from graviton-mediated inflaton annihilation, corresponding to the first diagram

in the second row of Fig. 3. We label the particle momenta as $\phi(p_1)\phi(p_2) \rightarrow h_{\mu\nu}(q) \rightarrow \chi(p_3)\bar{\chi}(p_4)$. The relevant vertices are given by [26]

$$-\frac{i}{M_P} [p_{1\mu} p_{2\nu} + p_{1\nu} p_{2\mu} - \eta_{\mu\nu} (p_1 \cdot p_2 + m_\phi^2)] \quad (\text{A.1})$$

for $\phi\phi h_{\mu\nu}$, and

$$-\frac{i}{4M_P} [(p_3 - p_4)_\mu \gamma_\nu + (p_3 - p_4)_\nu \gamma_\mu - 2\eta_{\mu\nu} (\not{p}_3 - \not{p}_4 - 2m_\chi)] \quad (\text{A.2})$$

for $\bar{\chi}\chi h_{\mu\nu}$. The graviton propagator reads

$$\Pi^{\mu\nu\rho\sigma} = \frac{1}{2q^2} (\eta^{\rho\nu}\eta^{\sigma\mu} + \eta^{\rho\mu}\eta^{\sigma\nu} - \eta^{\rho\sigma}\eta^{\mu\nu}). \quad (\text{A.3})$$

From these Feynman rules, we readily obtain the squared matrix element

$$\sum_{s_3, s_4} |\mathcal{M}|^2 = \frac{1}{2M_P^4} m_\chi^2 (m_\phi^2 - m_\chi^2), \quad (\text{A.4})$$

where s_3, s_4 denotes the spins of the final states. With the matrix element at hand, we arrive at the final result for the interaction-rate density

$$\gamma = \frac{\rho_\phi^2}{m_\phi^2} \frac{m_\chi^2}{64\pi M_P^4} \left(1 - \frac{m_\chi^2}{m_\phi^2}\right)^{3/2}. \quad (\text{A.5})$$

References

- [1] A.A. Starobinsky, *A New Type of Isotropic Cosmological Models Without Singularity*, *Phys. Lett. B* **91** (1980) 99.
- [2] A.H. Guth, *The Inflationary Universe: A Possible Solution to the Horizon and Flatness Problems*, *Phys. Rev. D* **23** (1981) 347.
- [3] A.D. Linde, *A New Inflationary Universe Scenario: A Possible Solution of the Horizon, Flatness, Homogeneity, Isotropy and Primordial Monopole Problems*, *Phys. Lett. B* **108** (1982) 389.
- [4] A. Albrecht and P.J. Steinhardt, *Cosmology for Grand Unified Theories with Radiatively Induced Symmetry Breaking*, *Phys. Rev. Lett.* **48** (1982) 1220.
- [5] J. Martin, C. Ringeval and V. Vennin, *Encyclopædia Inflationaris*, *Phys. Dark Univ.* **5-6** (2014) 75 [1303.3787].
- [6] PLANCK collaboration, *Planck 2018 results. X. Constraints on inflation*, *Astron. Astrophys.* **641** (2020) A10 [1807.06211].
- [7] BICEP2, KECK ARRAY collaboration, *BICEP2 / Keck Array x: Constraints on Primordial Gravitational Waves using Planck, WMAP, and New BICEP2/Keck Observations through the 2015 Season*, *Phys. Rev. Lett.* **121** (2018) 221301 [1810.05216].
- [8] H.M. Hodges, G.R. Blumenthal, L.A. Kofman and J.R. Primack, *Nonstandard Primordial Fluctuations From a Polynomial Inflaton Potential*, *Nucl. Phys. B* **335** (1990) 197.

- [9] R. Allahverdi, K. Enqvist, J. García-Bellido and A. Mazumdar, *Gauge invariant MSSM inflaton*, *Phys. Rev. Lett.* **97** (2006) 191304 [[hep-ph/0605035](#)].
- [10] C. Destri, H.J. de Vega and N.G. Sanchez, *MCMC analysis of WMAP3 and SDSS data points to broken symmetry inflaton potentials and provides a lower bound on the tensor to scalar ratio*, *Phys. Rev. D* **77** (2008) 043509 [[astro-ph/0703417](#)].
- [11] K. Nakayama, F. Takahashi and T.T. Yanagida, *Polynomial Chaotic Inflation in the Planck Era*, *Phys. Lett. B* **725** (2013) 111 [[1303.7315](#)].
- [12] K. Nakayama, F. Takahashi and T.T. Yanagida, *Polynomial Chaotic Inflation in Supergravity*, *JCAP* **08** (2013) 038 [[1305.5099](#)].
- [13] R. Kallosh, A. Linde and A. Westphal, *Chaotic Inflation in Supergravity after Planck and BICEP2*, *Phys. Rev. D* **90** (2014) 023534 [[1405.0270](#)].
- [14] T. Li, Z. Sun, C. Tian and L. Wu, *The Renormalizable Three-Term Polynomial Inflation with Large Tensor-to-Scalar Ratio*, *Eur. Phys. J. C* **75** (2015) 301 [[1407.8063](#)].
- [15] G. Aslanyan, L.C. Price, J. Adams, T. Bringmann, H.A. Clark, R. Easther et al., *Ultracompact minihalos as probes of inflationary cosmology*, *Phys. Rev. Lett.* **117** (2016) 141102 [[1512.04597](#)].
- [16] T.-J. Gao and Z.-K. Guo, *Inflection point inflation and dark energy in supergravity*, *Phys. Rev. D* **91** (2015) 123502 [[1503.05643](#)].
- [17] N. Musoke and R. Easther, *Expectations for Inflationary Observables: Simple or Natural?*, *JCAP* **12** (2017) 032 [[1709.01192](#)].
- [18] M. Drees and Y. Xu, *Small field polynomial inflation: reheating, radiative stability and lower bound*, *JCAP* **09** (2021) 012 [[2104.03977](#)].
- [19] M. Drees and Y. Xu, *Large field polynomial inflation: parameter space, predictions and (double) eternal nature*, *JCAP* **12** (2022) 005 [[2209.07545](#)].
- [20] Y. Xu, *Polynomial Inflation and Its Aftermath*, Ph.D. thesis, U. Bonn (main), 2022.
- [21] M. Drees and Y. Xu, *Parameter space of leptogenesis in polynomial inflation*, *JCAP* **04** (2024) 036 [[2401.02485](#)].
- [22] N. Bernal and Y. Xu, *Polynomial inflation and dark matter*, *Eur. Phys. J. C* **81** (2021) 877 [[2106.03950](#)].
- [23] F.L. Bezrukov and M. Shaposhnikov, *The Standard Model Higgs boson as the inflaton*, *Phys. Lett. B* **659** (2008) 703 [[0710.3755](#)].
- [24] R. Kallosh, A. Linde and D. Roest, *Superconformal Inflationary α -Attractors*, *JHEP* **11** (2013) 198 [[1311.0472](#)].
- [25] S. Izumine and K. Nakayama, *Effects of gravitational particle production on Higgs portal dark matter*, [2403.05199](#).
- [26] S.Y. Choi, J.S. Shim and H.S. Song, *Factorization and polarization in linearized gravity*, *Phys. Rev. D* **51** (1995) 2751 [[hep-th/9411092](#)].
- [27] D.H. Lyth and A.R. Liddle, *The primordial density perturbation: Cosmology, inflation and the origin of structure* (2009).
- [28] A.R. Liddle and S.M. Leach, *How long before the end of inflation were observable perturbations produced?*, *Phys. Rev. D* **68** (2003) 103503 [[astro-ph/0305263](#)].

- [29] PLANCK collaboration, *Planck 2018 results. VI. Cosmological parameters*, *Astron. Astrophys.* **641** (2020) A6 [[1807.06209](#)].
- [30] BICEP, KECK collaboration, *Improved Constraints on Primordial Gravitational Waves using Planck, WMAP, and BICEP/Keck Observations through the 2018 Observing Season*, *Phys. Rev. Lett.* **127** (2021) 151301 [[2110.00483](#)].
- [31] K. Abazajian et al., *CMB-S4 Science Case, Reference Design, and Project Plan*, [1907.04473](#).
- [32] R. Allahverdi, R. Brandenberger, F.-Y. Cyr-Racine and A. Mazumdar, *Reheating in Inflationary Cosmology: Theory and Applications*, *Ann. Rev. Nucl. Part. Sci.* **60** (2010) 27 [[1001.2600](#)].
- [33] M.A. Amin, M.P. Hertzberg, D.I. Kaiser and J. Karouby, *Nonperturbative Dynamics Of Reheating After Inflation: A Review*, *Int. J. Mod. Phys. D* **24** (2014) 1530003 [[1410.3808](#)].
- [34] K. Harigaya and K. Mukaida, *Thermalization after/during Reheating*, *JHEP* **05** (2014) 006 [[1312.3097](#)].
- [35] J. Ellis, M.A.G. García, D.V. Nanopoulos, K.A. Olive and M. Peloso, *Post-Inflationary Gravitino Production Revisited*, *JCAP* **03** (2016) 008 [[1512.05701](#)].
- [36] M.A.G. García and M.A. Amin, *Prethermalization production of dark matter*, *Phys. Rev. D* **98** (2018) 103504 [[1806.01865](#)].
- [37] S. Sarkar, *Big bang nucleosynthesis and physics beyond the standard model*, *Rept. Prog. Phys.* **59** (1996) 1493 [[hep-ph/9602260](#)].
- [38] M. Kawasaki, K. Kohri and N. Sugiyama, *MeV scale reheating temperature and thermalization of neutrino background*, *Phys. Rev. D* **62** (2000) 023506 [[astro-ph/0002127](#)].
- [39] S. Hannestad, *What is the lowest possible reheating temperature?*, *Phys. Rev. D* **70** (2004) 043506 [[astro-ph/0403291](#)].
- [40] F. De Bernardis, L. Pagano and A. Melchiorri, *New constraints on the reheating temperature of the universe after WMAP-5*, *Astropart. Phys.* **30** (2008) 192.
- [41] P.F. de Salas, M. Lattanzi, G. Mangano, G. Miele, S. Pastor and O. Pisanti, *Bounds on very low reheating scenarios after Planck*, *Phys. Rev. D* **92** (2015) 123534 [[1511.00672](#)].
- [42] G.F. Giudice, E.W. Kolb and A. Riotto, *Largest temperature of the radiation era and its cosmological implications*, *Phys. Rev. D* **64** (2001) 023508 [[hep-ph/0005123](#)].
- [43] J.F. Dufaux, G.N. Felder, L. Kofman, M. Peloso and D. Podolsky, *Preheating with trilinear interactions: Tachyonic resonance*, *JCAP* **07** (2006) 006 [[hep-ph/0602144](#)].
- [44] S. Cléry, Y. Mambrini, K.A. Olive and S. Verner, *Gravitational portals in the early Universe*, *Phys. Rev. D* **105** (2022) 075005 [[2112.15214](#)].
- [45] M.R. Haque and D. Maity, *Gravitational reheating*, *Phys. Rev. D* **107** (2023) 043531 [[2201.02348](#)].
- [46] B. Barman, S. Cléry, R.T. Co, Y. Mambrini and K.A. Olive, *Gravity as a portal to reheating, leptogenesis and dark matter*, *JHEP* **12** (2022) 072 [[2210.05716](#)].
- [47] M.R. Haque, D. Maity and R. Mondal, *Gravitational neutrino reheating*, *Phys. Rev. D* **109** (2024) 063543 [[2311.07684](#)].
- [48] S. Cléry, Y. Mambrini, K.A. Olive, A. Shkerin and S. Verner, *Gravitational portals with nonminimal couplings*, *Phys. Rev. D* **105** (2022) 095042 [[2203.02004](#)].

- [49] B. Barman, N. Bernal and J. Rubio, *Rescuing gravitational-reheating in chaotic inflation*, *JCAP* **05** (2024) 072 [[2310.06039](#)].
- [50] PARTICLE DATA GROUP collaboration, *Review of Particle Physics*, *PTEP* **2020** (2020) 083C01.
- [51] I. Masina, *Dark matter and dark radiation from evaporating primordial black holes*, *Eur. Phys. J. Plus* **135** (2020) 552 [[2004.04740](#)].
- [52] Y. Mambrini and K.A. Olive, *Gravitational Production of Dark Matter during Reheating*, *Phys. Rev. D* **103** (2021) 115009 [[2102.06214](#)].
- [53] N. Bernal and C.S. Fong, *Dark matter and leptogenesis from gravitational production*, *JCAP* **06** (2021) 028 [[2103.06896](#)].
- [54] B. Barman and N. Bernal, *Gravitational SIMPs*, *JCAP* **06** (2021) 011 [[2104.10699](#)].
- [55] B. Barman, N. Bernal, Y. Xu and Ó. Zapata, *Ultraviolet freeze-in with a time-dependent inflaton decay*, *JCAP* **07** (2022) 019 [[2202.12906](#)].
- [56] M. Garny, M. Sandora and M.S. Sloth, *Planckian Interacting Massive Particles as Dark Matter*, *Phys. Rev. Lett.* **116** (2016) 101302 [[1511.03278](#)].
- [57] Y. Tang and Y.-L. Wu, *On Thermal Gravitational Contribution to Particle Production and Dark Matter*, *Phys. Lett. B* **774** (2017) 676 [[1708.05138](#)].
- [58] M. Garny, A. Palessandro, M. Sandora and M.S. Sloth, *Theory and Phenomenology of Planckian Interacting Massive Particles as Dark Matter*, *JCAP* **02** (2018) 027 [[1709.09688](#)].
- [59] N. Bernal, M. Dutra, Y. Mambrini, K. Olive, M. Peloso and M. Pierre, *Spin-2 Portal Dark Matter*, *Phys. Rev. D* **97** (2018) 115020 [[1803.01866](#)].
- [60] M. Quiros, *Finite temperature field theory and phase transitions*, in *ICTP Summer School in High-Energy Physics and Cosmology*, pp. 187–259, 1, 1999 [[hep-ph/9901312](#)].
- [61] B. Barman, N. Bernal and Y. Xu, *Resonant Reheating*, [2404.16090](#).
- [62] N. Bernal, A. Donini, M.G. Folgado and N. Rius, *Kaluza-Klein FIMP Dark Matter in Warped Extra-Dimensions*, *JHEP* **09** (2020) 142 [[2004.14403](#)].
- [63] N. Bernal, A. Donini, M.G. Folgado and N. Rius, *FIMP Dark Matter in Clockwork/Linear Dilaton Extra-Dimensions*, *JHEP* **04** (2021) 061 [[2012.10453](#)].